Cell Reports, Volume *43*

Supplemental information

Functional organization of posterior parietal cortex circuitry based on inferred information flow

Jung Uk Kang, Eric Mooshagian, and Lawrence H. Snyder

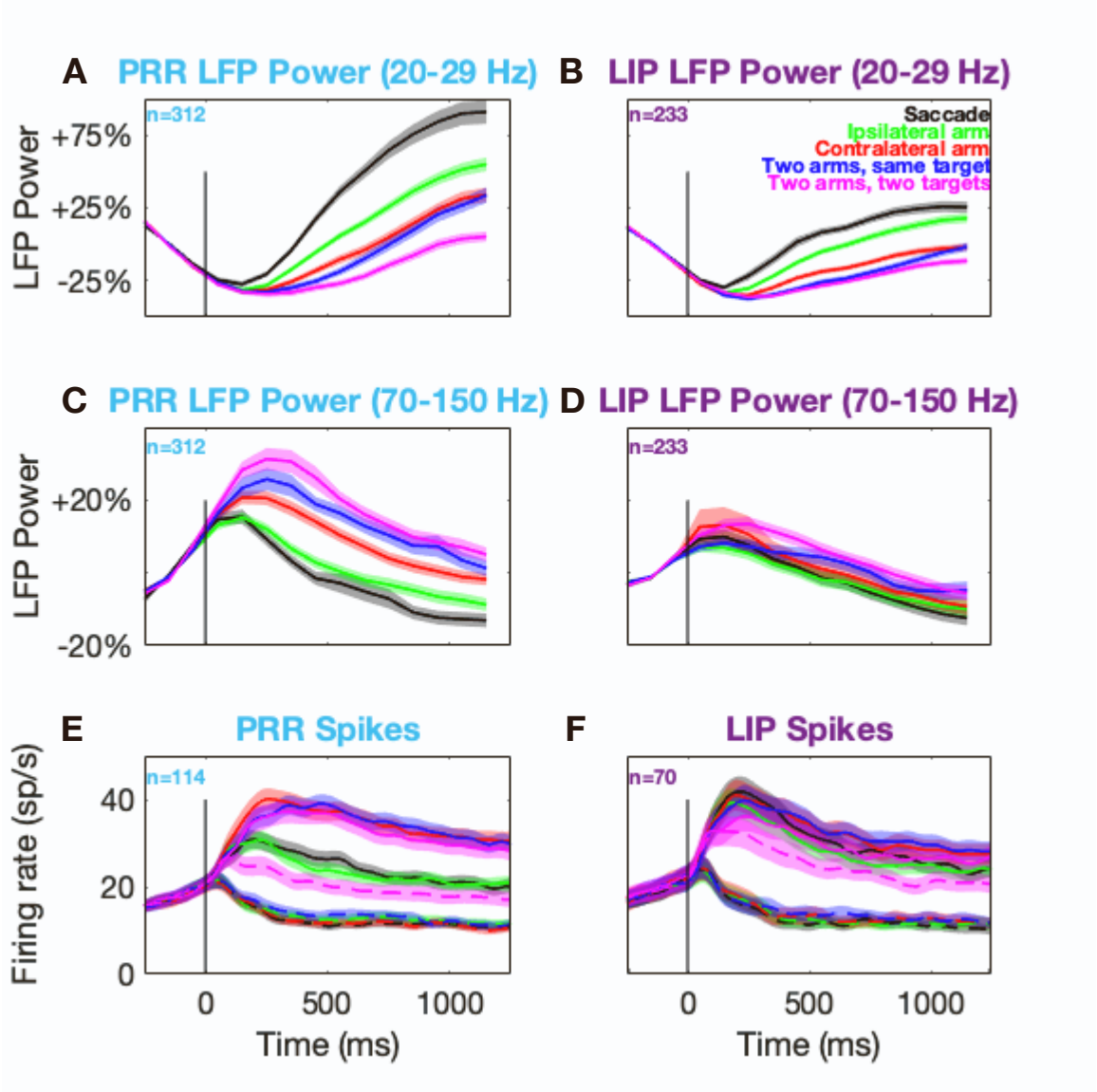

Figure S1. Spikes and LFP power from PRR and LIP aligned to target onset

(A) LFP power in PRR at 20-29 Hz. Solid lines denote preferred direction responses. Shaded regions denote ±1 SEM.

(B) LFP power in LIP at 20-29 Hz.

(C) LFP power in PRR at 70-150 Hz.

(D) LFP power in LIP at 70-150 Hz.

(E) Spikes in PRR. Dotted lines in denote null direction responses.

(F) Spikes in LIP.

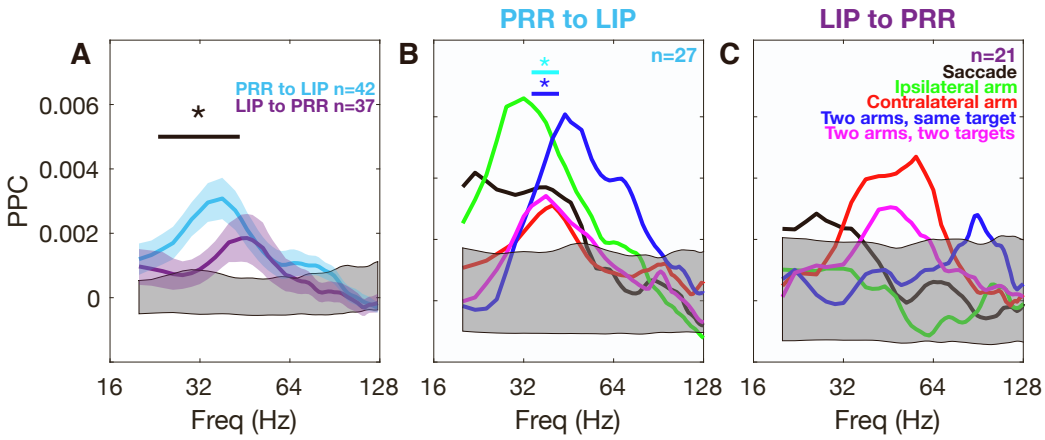

Figure S2. Spike-LFP pairwise phase consistency (PPC) between PRR and LIP within hemisphere

(A) Format identical to Figure 2B. For both directions of communication (from PRR to LIP and from LIP to PRR), we computed spike-LFP PPC after combining the four reaching tasks during the planning period. PRR to LIP PPC is significantly higher than vice versa at 24-42 Hz. Peak PRR-to-LIP PPC is 0.031 at 38 Hz, while peak LIP-to-PRR PPC is 0.019 at 46 Hz. Measured from the chance level of 0.000, this is a ratio of greater than 1.6:1. The grey shaded regions represent the 99% bounds of a shuffle test. Colored shaded regions denote ±1 SEM. The black asterisk and straight line denote $p < 0.001$ (pooled t-test). PPC compensates for the number of spikes so that, unlike coherence, it is not a biased statistic. For this reason, we included data from all spike-LFP pairs regardless of spike count in this and subsequent panels.

(B-C) For each direction of communication (from PRR to LIP and from LIP to PRR, respectively), we compute spike-LFP PPC for each task type at each frequency during the planning period of coordinated eye and arm movements. The grey shaded regions represent the 99% bounds of a shuffle test.

(B) From PRR to LIP. Blue and cyan asterisks and straight lines indicate frequencies (34-42 Hz) with significant differences in PPC modulation in all five tasks and the four tasks that involve reaching, respectively (repeated-measures ANOVA [$p < 0.01$]).

(C) From LIP to PRR. No significant task-specific modulation in PPC.

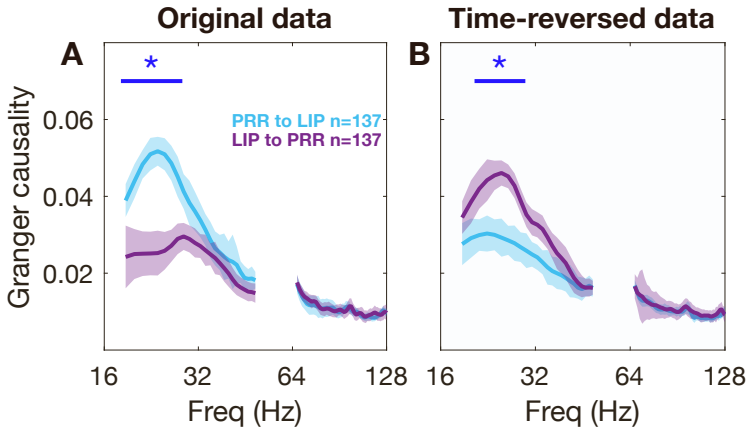

Figure S3. Time-reversal analysis of spectral Granger causality between PRR and LIP

Time reversal should invert the order of the two traces. If this is not the case, then Granger causality results are likely due to an artifact such as greater power in one signal than the other. In both panels, colored shaded regions denote ±1 SEM. The blue asterisks and straight lines denote $p < 0.001$ (Wilcoxon signed-rank test).

(A) Granger causality from original data in during the planning period of coordinated eye and arm movements, 800 ms prior to the cue to initiate movement. Granger causality from PRR to LIP is significantly higher than Granger causality from LIP to PRR at 19-27 Hz.

(B) Granger causality from time-reversed data. With time-reversal, Granger causality from PRR to LIP is significantly lower than Granger causality from LIP to PRR at 21 to 29 Hz. Peak PRR-to-LIP Granger causality was 0.030 at 22 Hz, while peak LIP-to-PRR Granger causality was 0.046 at 25 Hz. This suggests that the observed effect is legitimate rather than due to artifact. In contrast, effects below 16 Hz were not inverted (data not shown), indicating that Granger causality from these low frequencies is unreliable.

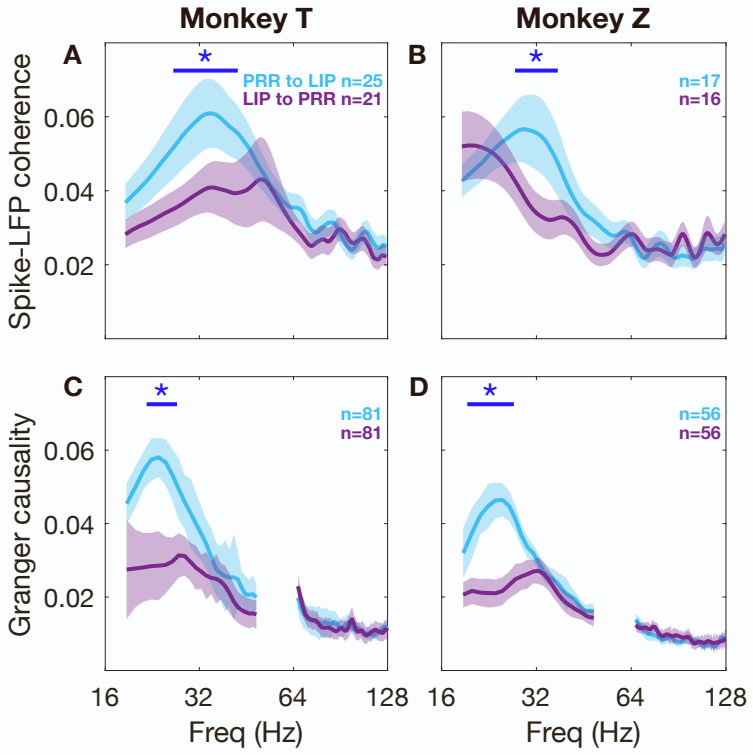

Figure S4. Results from individual animals

(A and B) Within hemisphere spike-LFP coherence for individual animals. Format same as in Figure 2B.

(C and D) Within hemisphere spectral Granger causality for individual animals. Format same as in Figure 2D.

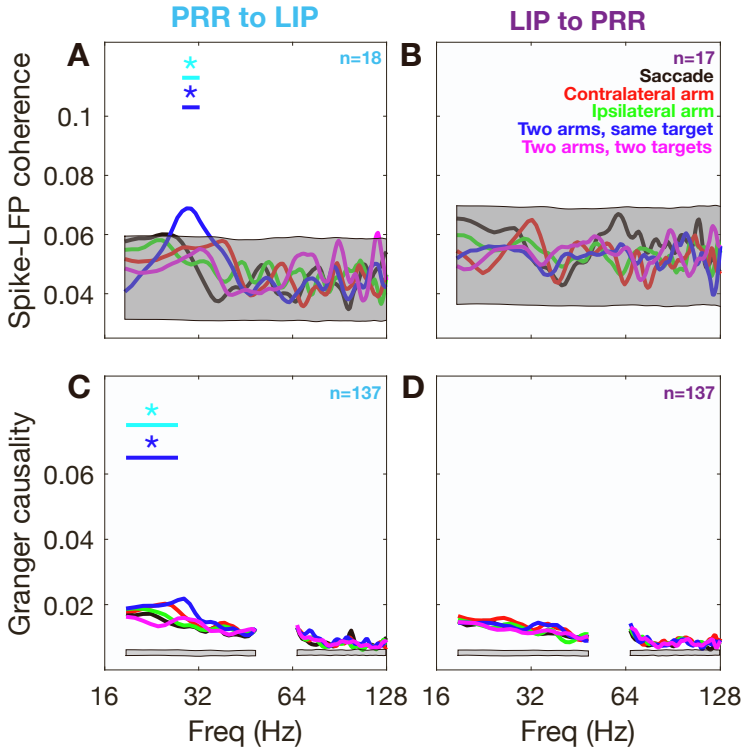

Figure S5. Information flow is task-specific from PRR to LIP across hemispheres

Spike-LFP coherence is shown above (A-B), and spectral Granger causality below (C-D). The grey shaded regions represent the 99% bounds of a shuffle test. Cyan and blue asterisks and straight lines indicate frequencies with a significant difference in modulation across four reach tasks and all five tasks, respectively (repeated-measures ANOVA [$p < 0.001$] for spike-LFP coherence, and a permutation test [$p < 0.01$] for spectral Granger causality).

(A) Spike-LFP coherence from PRR to LIP. The effects are not strong; only the two arms, same target task (blue) has a peak at 0.069 at 29 Hz above the 99% upper bound of the grey shaded region. However, there is a significant task-specific modulation at 28-32 Hz.

(B) Spike-LFP coherence from LIP to PRR. All spike-LFP coherence values are within the 99% bounds of the grey shaded region. No task-specific modulation.

(C) Granger causality from PRR to LIP. There is task-specific modulation at 19-27 Hz. Peak values in Granger causality from PRR to LIP are at 20-30 Hz: saccade (black) at 0.017 at 22 Hz, contralateral arm (red) at 0.020 at 25 Hz. ipsilateral arm at 0.019 at 20 Hz, two arms, same target (blue) at 0.022 at 29 Hz, and two arms, different targets at (magenta) at 0.016 at 19 Hz.

(D) No task-specific modulation in Granger causality from LIP to PRR.

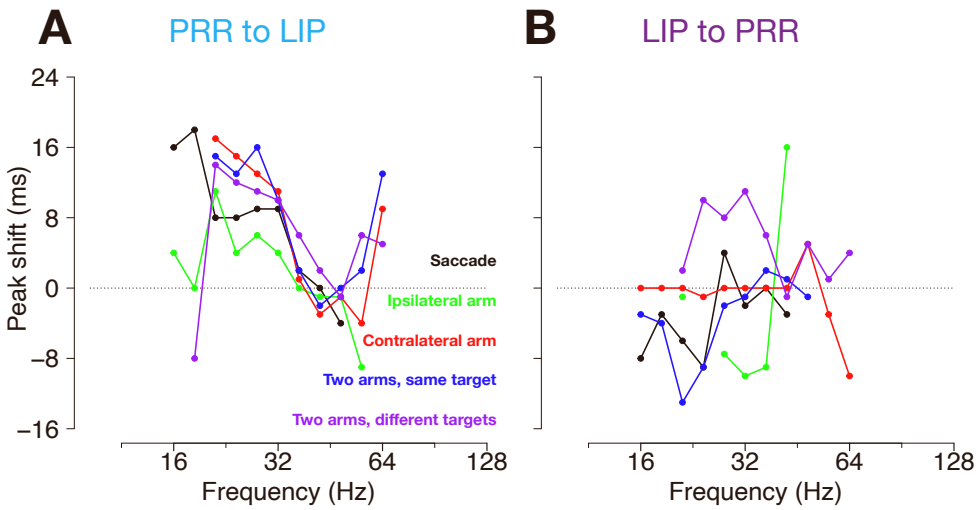

Figure S6. Timed-lagged spike-LFP coherence analysis across different frequencies in each task

For each direction of communication (from PRR to LIP and from LIP to PRR within hemisphere, respectively), we ran the time-lagged spike-LFP coherence analysis for each task type in each frequency and computed a peak time shift (ms) with respect to LFPs. Frequencies with no clear peak are omitted.

(A) From PRR to LIP. At 21-36 Hz, saccade (black) and ipsilateral reach (green) have lower peaks of ~8 ms. The other task types which include contralateral reach (red, blue, purple) have peaks of ~12 ms.

(B) From LIP to PRR. At 21-36 Hz, bimanual movements to different targets (purple) have a peak of ~8 ms and contralateral reach (red) has no consistent lag or lead. The other task types (black, blue, green) have a lead of ~8 ms, which is consistent with common input.

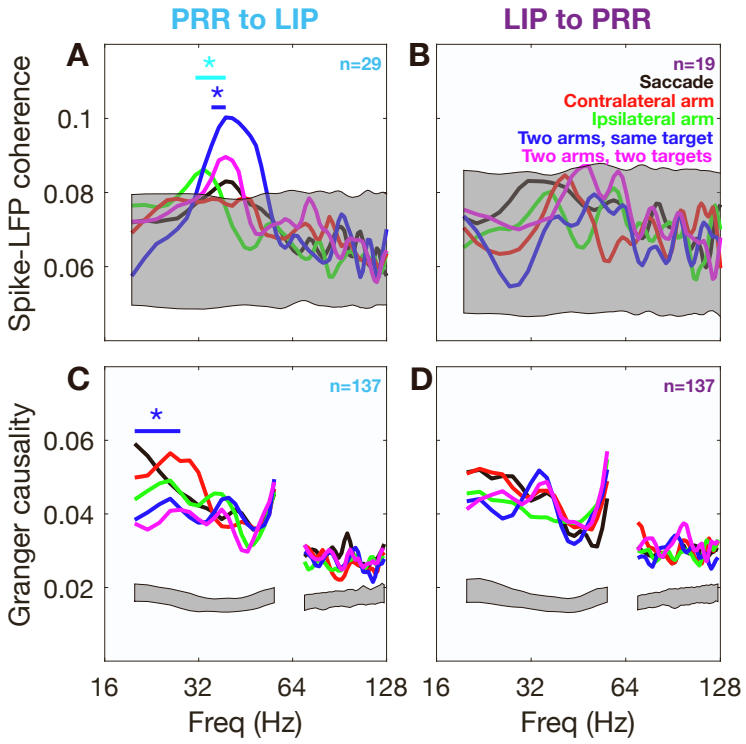

Figure S7. Information flow 50-550 ms after target onset on coordinated eye and arm movement trials (colored) and eye movement only trials (black)

Spike-LFP coherence is shown above (A-B), spectral Granger causality below (C-D). Flow from PRR to LIP is shown on the left and from LIP to PRR on the right. The lower grey shaded region represents the 99% bound of a shuffle test. Cyan and blue asterisks and straight lines indicate frequencies with a significant difference in modulation by four reach tasks and all five tasks, respectively (repeated-measures ANOVA [$p < 0.001$] for spike-LFP coherence, and a permutation test [$p < 0.01$] for spectral Granger causality).

(A) Spike-LFP coherence from PRR to LIP. Peak coherence values were at 39 Hz: 0.083 (saccade, black), 0.100 (two arms, same target, blue), and 0.090 (two arms, different targets, magenta). Ipsilateral arm movements (green) have a peak at 0.086 at 33 Hz. There is a significant task-specific modulation across four reach task types and all five task types at 31-39 Hz (cyan asterisk) and 35-39 Hz (blue asterisk), respectively.

(B) No task-specific modulation in spike-LFP coherence from LIP to PRR. All coherence values are within the 99% bounds of the grey shaded area.

(C) Granger causality from PRR to LIP. Granger causality from PRR to LIP has significant task-specific modulation at 19-27 Hz across four reach task types ($p < 0.01$, blue asterisk) and all five task types ($p < 0.02$). Peak coherence for saccade-only (black) is at 0.059 at 20 Hz. All four reach task types have their respective peak coherence values at 26 Hz: 0.056 (red), 0.049 (green), 0.053 (blue), and 0.041 (magenta).

(D) No task-specific modulation in Granger causality from LIP to PRR. Bimanual movement task types (blue and magenta) have their peaks at 0.052 at 34 Hz and 0.948 at 36 Hz, respectively. Saccade and unimanual movement task types have their respective peaks at 22 Hz: 0.052 (black and red) and 0.046 (green).

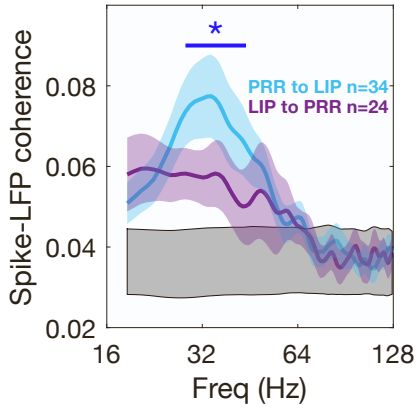

Figure S8. Coherence between spikes associated with the preferred direction and LFP between PRR and LIP within hemisphere

For this analysis, only spikes from preferred direction trials were used. Results are similar to those using all directions. PRR to LIP coherence is significantly higher than vice versa at 28-44 Hz. The blue asterisk and straight line denote $p < 0.001$ (pooled t-test). Peak PRR-to-LIP coherence is 0.077 at 34 Hz, while peak LIP-to-PRR coherence is 0.060 at 21 Hz. Measured from the chance level of 0.036, this is a ratio of greater than 1.7:1. Colored shaded regions denote ±1 SEM. The lower grey shaded region represents the 99% bounds of a shuffle test.

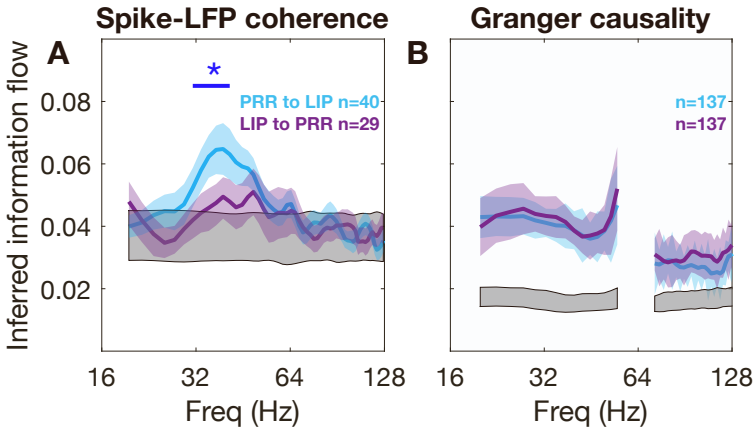

Figure S9. Inferred information flow between PRR and LIP during the target presentation period (50:450 ms aligned to the target onset) for coordinated eye and arm movements

(A) Spike-LFP coherence between PRR and LIP in the same hemisphere. Peak PRR-to-LIP coherence was 0.065 at 39 Hz, while peak LIP-to-PRR coherence was 0.050 at 39 Hz. Measured from the chance level of 0.036, this is a ratio of greater than 2:1. The colored shaded regions denote ±1 SEM. The lower grey shaded region represents the 99% bounds from a shuffle test. The blue asterisk and straight line denote $p < 0.001$ (pooled t-test). Granger causality from PRR to LIP was significantly higher than vice versa at 31 to 42 Hz. In a shorter target presentation period (50:350 ms aligned to the target onset), spike-LFP coherence from PRR to LIP was higher than vice versa at 27 to 37 Hz (pooled t-test [$p < 0.01$]).

(B) Spectral Granger causality between PRR and LIP in the same hemisphere. No significant differences between information flow between the two directions.

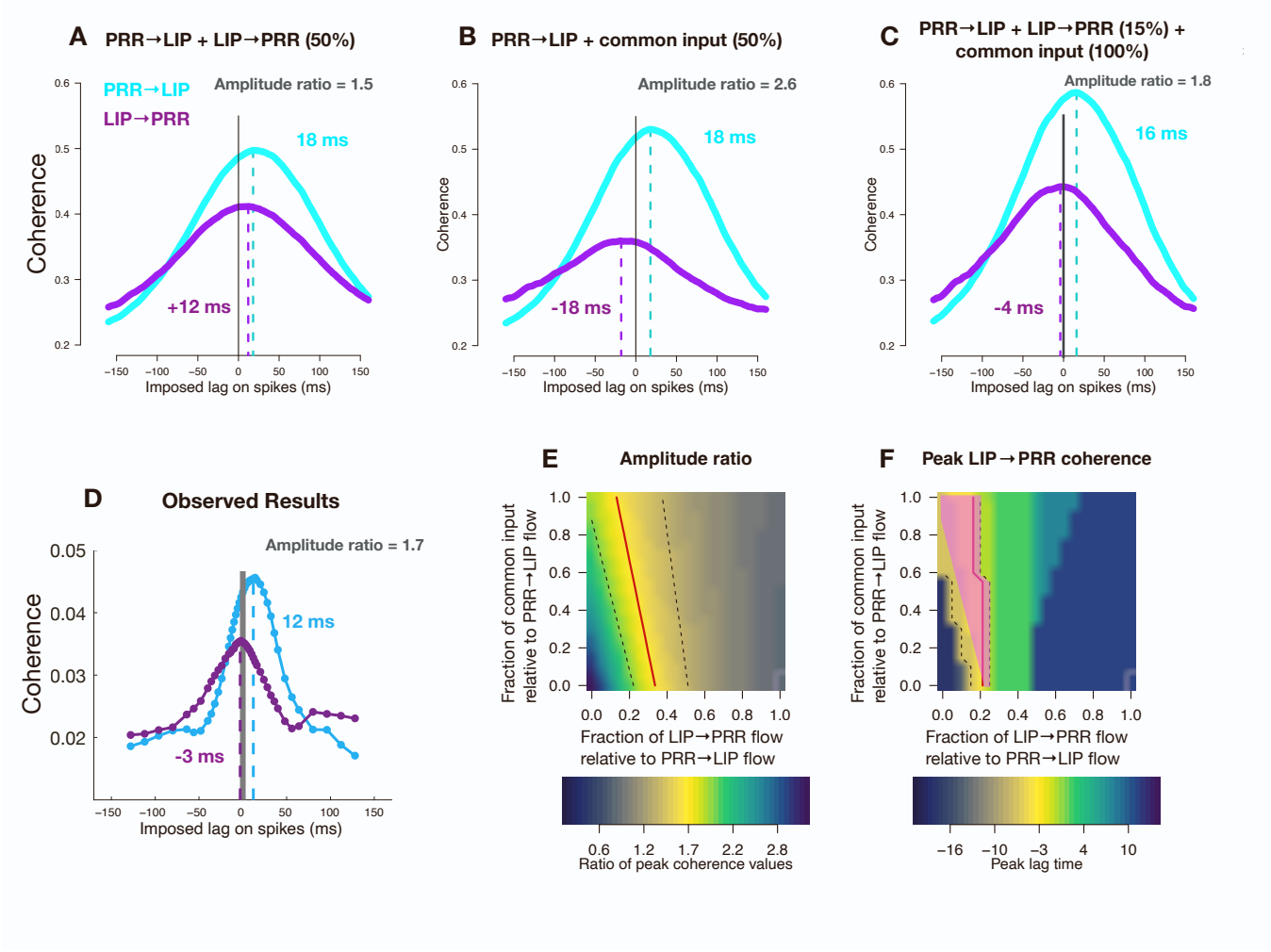

Figure S10. Similar results from time-lagged coherence analysis of different simulated combinations of information flow

(A) Time-lagged spike-LFP coherence analysis. A simulation of information flow from PRR to LIP plus information flow from LIP to PRR that is only half as strong fails to replicate the negative peak lag time for LIP to PRR coherence seen in the experimental data (Figure 5E, replicated here in D).

(B) If PRR to LIP flow is combined instead with common input, the peak lag for coherence from LIP to PRR becomes negative, but the lag is too large (-18 ms in the simulation versus -3 ms in the observed data) and the amplitude is too weak (PRR to LIP coherence is 2.6 times larger for LIP to PRR coherence in the simulation, compared to 1.7 times larger in the observed results).

(C) A combination of LIP to PRR signal flow that is 15% as large as the PRR to LIP flow, plus strong common input to both areas, replicates both the peak lag and the relative amplitude of the observed LIP to PRR coherence (-4 ms and a ratio of 1.8, compared to -3 ms and 1.7).

(E) and (F) show the amplitude ratio and time of peak lag for the LIP to PRR coherence measurement found in the simulated data, as a function of the amounts of common input (ordinate) and LIP to PRR flow (abscissa). Each are expressed as a fraction of the PRR to LIP flow. The color scales are adjusted so that the values observed in the experimental data are shown in yellow. These values are emphasized by a red line flanked by dashed lines. The dashed lines are at amplitudes of ± 20% of the observed amplitude and ±3 ms of the observed peak lag time. The intersection of the areas enclosed by dashes in the two panels, shown in pink in (F), represents the information flow that best replicates

the observed data. Thus, the simulation suggests flow from LIP to PRR during a coordinated reach is at best only 1/5th as strong as flow from PRR to LIP, and could be even smaller, depending on the amount of common input to the two areas.

Inasmuch as the simulated effects shown are similar to the experimental results obtained in the current study (Figures 5E and 6), we conclude that the dominant information flow during the delay period of a coordinated reach task is from PRR to LIP. There may or may not be flow from LIP to PRR, and there may or may not be common input. In any case, however, the maximum LIP-to-PRR flow is no more than 20% of PRR-to-LIP flow.

While the peak lags, amplitude ratios, and general form of the simulation results match the observed data, the scales are different. Coherence is an order of magnitude much stronger in the simulation, and the bandwidth time-lagged analysis plot is about twice as wide. We could adjust the parameters of the simulation for a closer match. For example, increasing model stochasticity would decrease coherence strength (see Methods). It is likely, however, that these differences in scale reflect the fact that the connectivity (fan-in and fan-out) in our simulation is one-to-one while the actual cortical connectivity is roughly one thousand to one, resulting in much lower coherence and perhaps sharpening the bandwidth as well. Exploring these issues is of significant interest but beyond the scope of the current study.